Journal of King Saud University – Computer and Information Sciences (2013) 25, 163–171

King Saud University

Journal of King Saud University – Computer and Information Sciences

www.ksu.edu.sa
www.sciencedirect.com

ORIGINAL ARTICLE

Multibit quantization index modulation: A high-rate robust data-hiding method

Amit Phadikar *

Department of Information Technology, MCKV Institute of Engineering, Liluah, Howrah 711204, India

Received 28 May 2012; revised 18 September 2012; accepted 11 November 2012
Available online 28 November 2012

KEYWORDS

Watermarking;
Multibit QIM;
M-ary amplitude modulation;
Lifting;
Robustness

Abstract Nowadays, the quantization index modulation (QIM) principle is popular in digital watermarking due to its considerable performance advantages over spread-spectrum and low-bit(s) modulation. In a QIM-based data-hiding scheme, it is a challenging task to embed multiple bits of information into the host signal. This work proposes a new model of QIM, i.e., the M-ary amplitude modulation principle for multibit watermarking. The watermark embedding process may be divided into two phases. In the first phase, a binary watermark image is spatially dispersed using a sequence of numbers generated by a secret key. In the second phase, the host image is decomposed by lifting, and the encoded watermark bits are embedded into the high–low (HL) and low–high (LH) subbands of DWT-coefficients using M-ary amplitude modulation. The results of the simulation show that the robustness increases, at the cost of increased decoding complexity, for a high M-value. Furthermore, this investigation has shown that the decoding complexity of higher M-values can be overcome at moderate N-values, while the robustness performance is maintained at satisfactory level.

1. Introduction

Quantization index modulation (QIM) has recently become a popular form of watermarking based on the framework of communication with side information (Costa, 1983). A QIM-based technique embeds information by quantizing the original sample values. Typical QIM is accomplished by modulating a signal with the embedded information. Quantization is then performed using the associated quantizer. To improve on the performance of traditional QIM, a number of variants of the basic QIM algorithm, namely distortion-compensated dither modulation (DC-QIM) (Chen and Wornell, 2001), spread transform dither modulation (STDM) (Chen and Wornell, 2001), rational dither modulation (RDM) (Gonzalez et al., 2005), adaptive QIM using modified Watson distance (QIM-MW) and adaptive RDM using a modified Watson distance (RDM-MW) have been proposed. Moreover, various channel coding schemes and the M-ary modulation technique can also be used for performance improvement, as they are widely used in digital communication to increase data transmission reliability. While a channel-coding scheme reduces the data transmission rate to improve reliability, the M-ary

* Tel.: +91 33 2654 9315; fax: +91 33 2654 9318.
E-mail address: amitphadikar@rediffmail.com.
Peer review under responsibility of King Saud University.

1319-1578 © 2013 Production and hosting by Elsevier B.V. on behalf of King Saud University.
http://dx.doi.org/10.1016/j.jksuci.2012.11.005

principle of modulation improves detection performance by increasing the number of transmitted symbols.

The objective of this work is to design a new model of QIM for a multibit image-watermarking scheme based on our previous work (Phadikar and Maity, 2010). We have done our best to minimize the overlap between this work and the conference paper (Phadikar and Maity, 2010), offering more thorough insights and a report of our model's performance against various signal processing and attack operations, including a Rayleigh fading wireless channel. The overall objective is achieved by designing an M-ary amplitude modulation system based on a near-orthogonal dither. The encoded watermark bits are embedded into DWT-coefficients using the M-ary amplitude modulation technique. The multi-resolution nature of wavelets reflects the anisotropic properties of the human visual system (HVS) more precisely, which helps to design watermarking scheme, that is more robust against transmission and decoding errors. The superiority of the proposed scheme is verified by simulation results and compared with selected other methods.

The rest of the paper is organized as follows: Section 2 describes the system model for the proposed M-ary QIM. Section 3 describes the basic principles and key features of lifting-based DWT. Section 4 describes the proposed watermarking scheme. Section 5 presents some experimental results, and Section 6 describes our conclusions and the scope of future work.

2. System model for the proposed M-ary QIM

In digital communication, M-ary modulation offers bandwidth efficiency over binary transmission. The basic quantization index modulation (QIM) algorithm quantizes the feature vector X using a quantizer $Q_\Delta(.)$ chosen from a family of quantizers based on the message bit (m), to be embedded (Chen and Wornell, 2001). The watermarked featured vector $\tilde{X}$ is then obtained by:

$$\tilde{X} = Q_\Delta(X + d(m)) - d(m); m \in \{0, 1\} \tag{1}$$

where 'Δ' is a fixed quantization step size, and $d(.)$ is the dither used to embed the watermark bit. At the decoder, the test signal $\tilde{X}$ is requantized using the same family of quantizer to determine the embedded message bit, i.e.,

$$\hat{m} = arg \min_{m\in\{0,1\}} \sum_{i=1}^{L} \left| \tilde{X} - Q_\Delta(\tilde{X} + d(m)) - d(m) \right| \tag{2}$$

where we have the assumption that the scheme uses a soft decoder, and the symbol 'L' is the length of the dither.

In QIM-based watermarking, it is a challenging task to embed multiple bits of information into the same set of host samples by considering each watermark bit separately. Spread spectrum watermarking, more specifically code division multiple access (CDMA) watermarking, employs an orthogonal set of code patterns to embed multiple bits in the same set of host samples (Maity et al., 2005). This concept creates the possibility of exploring the use of orthogonal (or near-orthogonal) code patterns to create orthogonal (or near-orthogonal) dithers sets for QIM watermarking using M-ary amplitude modulation. In the literature, it has been shown that an M-ary modulation-based watermarking system significantly outperforms over a binary modulation-based watermarking system (Xin and Pawlak, 2008). In M-ary modulation, a group of symbols are treated as a single entity. We can relate the number of bits (N) and the number of different symbols (M) with the following equation:

$$M = 2^N \tag{3}$$

Obviously, the binary transmission system is a special case of an M-ary data transmission system. An effective method of implementing an M-ary amplitude modulation technique is based on a near-orthogonal dither. A group of near-orthogonal dithers $d \in \{d_0, d_1, ..., d_{M-1}\}$ is generated independently using the Hadamard function of a standard math library and a random number generated using a secret key (k). A Hadamard matrix is a square matrix whose entries are either $+1$ or -1. The smallest possible Hadamard matrix is of order two and is defined as

$$H_2 = \begin{bmatrix} 1 & 1 \\ 1 & -1 \end{bmatrix} \tag{4}$$

The Hadamard matrix with an order of a power of two may be constructed from H_2 based on the Kronecker product and given by

$$H_{2^m} = H_2 \otimes H_{2^{m-1}} = \begin{bmatrix} H_{2^{m-1}} & H_{2^{m-1}} \\ H_{2^{m-1}} & -H_{2^{m-1}} \end{bmatrix} \tag{5}$$

for $2 \leqslant m \in N$, where $\otimes$ denotes the Kronecker product. The symbol 'm' is a non-negative integer. Eq. (6) shows an example of a Hadamard matrix with order 4.

$$H_4 = \begin{bmatrix} H_2 & H_2 \\ H_2 & -H_2 \end{bmatrix} = \begin{bmatrix} 1 & 1 & 1 & 1 \\ 1 & -1 & 1 & -1 \\ 1 & 1 & -1 & -1 \\ 1 & -1 & -1 & 1 \end{bmatrix} \tag{6}$$

The basic characteristic of the Hadamard matrix is that all rows are orthogonal. The sequence of a random number is an *i.i.d.*, following a Gaussian distribution $\eta(0,1)$. The generation of the dither can be defined as follows:

$$d_i = H(\bullet) \times R \times \Delta/2 \tag{7}$$

where $H(\bullet)$ is the Hadamard function to generate the orthogonal code; Δ is the step size for dither modulation; and R is a random number generated using the following rule:

$$R = [\Re_L(k_1) + \Re_L(k_2) + \cdots + \Re_L(k_n)]/n \tag{8}$$

The function $\Re(k)$ is the random number generator. The symbol R is multiplied by $H(.)$ to increase the security of the system.

One of the prominent characteristics of the dithers generated in this manner is their near-orthogonal property, i.e.,

- d_i for $i = 1, 2\ldots, M$ should be distinct sequences.
- The inner product between d_i and itself would be the maximum, i.e., $\langle d_i, d_j \rangle$ should be the maximum.
- The spatial correlation $\langle d_i, d_j \rangle$, $i \neq j$ should be the minimum. Ideally, the sequences d_i and d_j should be orthogonal whenever $i \neq j$, i.e., $\langle d_i, d_j \rangle = 0$, $i \neq j$.
- Although the rows (and columns) of the Hadamard matrix are orthogonal, they are deterministic in nature. On the other hand, dithers so generated are not only (near-) orthogonal but also contain a form of randomness. Hence, their use in data hiding provides security by preventing the removal of embedded watermark followed by detection for the unauthorized users.

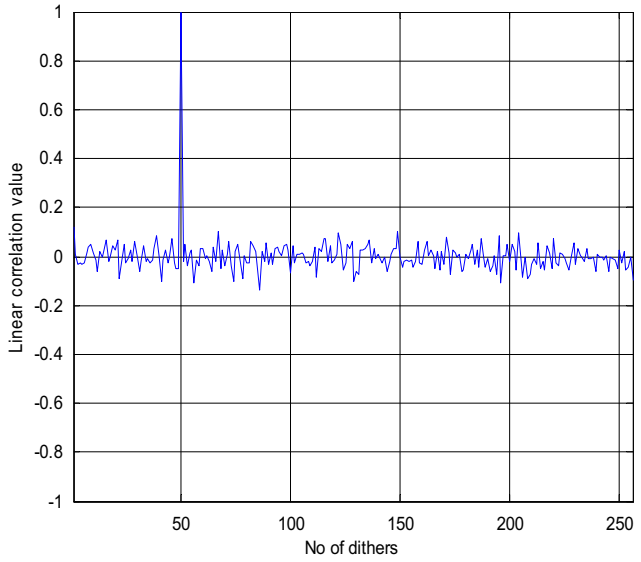

Figure 1 Linear correlation between a dither and its near-orthogonal version.

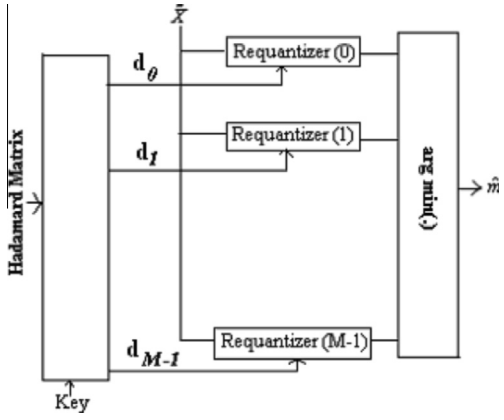

Figure 2 Structure of decoder for the extraction of M-ary watermark.

Those properties are illustrated in Fig. 1, where, as an example, d is a set of dithers with 256 elements, and the correlations of d_{50} with all the other dithers in the set are shown.

If each dither 'd' in the group is used to represent an M-ary message symbol $m \in \{0, 1, ..., M-1\}$, it consists of $\log_2 M = N$ bits of information once chosen for data embedding. With a QIM embedding function, the message 'm' can be embedded into the feature vector (X) according to the following rule:

$$\tilde{X} = Q_\Delta(X + d(m)) - d(m); m \in \{0, 1, ..., M-1\} \quad (9)$$

For watermark decoding, the same set of dithers $d \in \{d_0, d_1, ..., d_{M-1}\}$ is used. Fig. 2 shows the block diagram of the watermark decoding in an M-ary system. At the decoder, the test signal $\tilde{X}$ is requantized using the family of quantizers 'd' to determine the embedded message bit, i.e.,

$$\hat{m} = arg \min_{m \in \{0,1,..,M-1\}} \sum_{i=1}^{L} |\tilde{X} - Q_\Delta(\tilde{X} + d(m)) - d(m)| \quad (10)$$

In general, the greater the value of M, the better system performance in terms of robustness for a fixed capacity, with an increase in decoding complexity. In other words, for a fixed robustness, M-ary amplitude modulation offers higher capacity than binary modulation.

3. Basic principles and key features of lifting-based DWT

The lifting scheme is a technique for both designing fast wavelets and performing the discrete wavelet transform. The technique was introduced by Wim Sweldens. The discrete wavelet transform applies several filters separately to the same signal (Calderbank et al., 1998). The signal is divided like a zipper for the lifting scheme. Then, a series of convolution-accumulation operations are applied across the divided signals. Generally speaking, the lifting scheme includes three steps, splitting, prediction and update. The basic idea of lifting is described briefly below (Claypoole et al., 1998):

3.1. Split

The original signal is divided into two disjoint subsets. Although any disjoint split is possible, we will split the original data set $x[n]$ into $x_e[n] = x[2n]$, the even indexed points, and $x_o[n] = x[2n + 1]$, the odd indexed points.

3.2. Predict

The set of wavelet coefficients $d[n]$ is generated as an error in predicting $x_o[n]$ from $x_e[n]$ using the prediction operator P.

$$d[n] = x_o[n] + P(x_e[n]) \quad (11)$$

3.3. Update

$x_e[n]$ and $d[n]$ are combined to obtain scaling coefficients $c[n]$ that represent a coarse approximation to the original signal $x[n]$. This task is accomplished by applying an update operator U to the wavelet coefficients and adding the result to $x_e[n]$:

$$c[n] = x_e[n] + U(d[n]) \quad (12)$$

These three steps form a lifting stage. The iteration of the lifting stage on the output $c[n]$ creates the complete set of DWT scaling and wavelet coefficients $c^j[n]$ and $d^j[n]$. At each scale, we weight the $c^j[n]$ and $d^j[n]$ with k_e and k_o, respectively, as shown in Fig. 3. This process normalizes the energy of the underlying scaling and wavelet functions.

The lifting steps are easily inverted even if P and U are nonlinear, space-varying, or noninvertible. Rearranging Eqs. (11) and (12), we have

$$x_e[n] = c[n] - U(d[n]), x_o[n] = d[n] + P(x_e[n]) \quad (13)$$

The original signal will be perfectly reconstructed as long as the same P and U are chosen for the forward and the inverse transforms. The inverse lifting stage is shown in Fig. 4.

Moreover, in lifting, the odd sample values of the signal are updated with a weighted sum of the even sample values, and the even sample values are updated with a weighted sum of the odd sample values that allows the creation of correlation among the sample values (Boliek et al., 2000; Adams and Kossentini, 2000). This form of correlation may be beneficial for

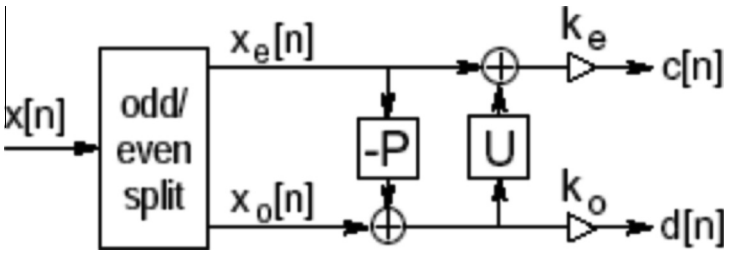

Figure 3 Lifting steps.

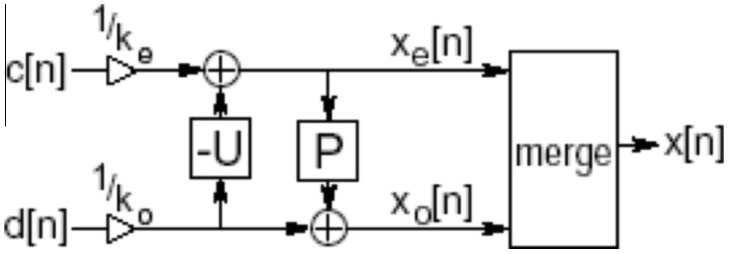

Figure 4 Typical inverse lifting steps.

Table 1 Entropy of different subbands for normal DWT and lifting.

	Low–low (LL)	High–low (HL)	Low–high (LH)	High–high (HH)
Lifting	7.26	5.24	5.42	5.40
DWT	10.41	8.30	6.78	8.62

data hiding on the coefficients and improves the visual image quality of the watermarked data. To support the above argument, we calculate the entropy of the different subbands for both traditional DWT and lifting. The average result is shown in Table 1. The lower values of entropy for lifting-based decomposition indicate that there exists a greater correlation between the coefficients in the lifting method than in the traditional DWT. Data hiding exploits the advantages of this redundancy to embed more bits of watermark for a given embedding distortion.

Lastly, the lifting scheme has several advantages over the classical wavelet based transform, which are described below (Uytterhoeven et al., 1997):

- Easy to understand and implement.
- Faster (×2, but still O (n), where n is the length of the signal).
- Inverse transform is easier to find.
- Inverse transform has exactly the same complexity as the forward transform.
- Transforms signals with an arbitrary length (need not be 2^n, where n is the length of the signal).
- Requires less memory.
- All wavelet filters can be implemented using the lifting scheme.
- Simple extensions to an integer transform are possible.

4. Proposed watermarking scheme

A block diagram of the proposed M-ary amplitude modulation-based QIM watermarking scheme is shown in Fig. 5.

4.1. Encoding process

The encoding process consists of the following steps:

Step 1: Watermark Permutation: A binary image that is chosen as a watermark is processed before embedding because the attacker can easily forge a watermark if he has the knowledge of it. Let the original binary image signature (W) and a $2-\mathrm{D}$ pseudorandom binary sequence K (which will be used as a secret key), each with size ($n' \times n'$), be described as follows:

$$W = \{w(i,j), 1 \leqslant i \leqslant n', 1 \leqslant j \leqslant n', w(i,j) \in \{0,1\}\} \tag{14}$$

$$K = \{k(i,j), 1 \leqslant i \leqslant n', 1 \leqslant j \leqslant n', k(i,j) \in \{0,1\}\} \tag{15}$$

The permuted watermark is calculated as follows:

$$W' = W \oplus K \tag{16}$$

where $\oplus$ denotes the XOR operation.

Step 2: Image Transformation and Selection of Subbands for Watermark Embedding: n-level lifting is performed on the original image. It has been shown in our previous work (Phadikar et al., 2008) that the integer wavelet provides superior performance compared to the classical DWT. This improvement is because the bit error rate (P_e) in binary watermark decoding is related to the standard deviation of the cover image coefficients (Voloshynovskiy and Pun, 2002) as follows:

$$P_e = \frac{2(M-1)}{M} \Upsilon\left(\sqrt{\frac{Nd_0^2}{4\sigma_x^2}}\right) \tag{17}$$

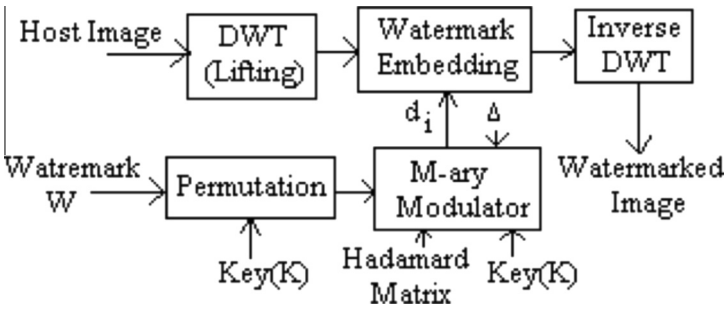

Figure 5 Block diagram of M-ary amplitude modulation based QIM watermarking scheme.

where d_0 indicates step size (Δ); M indicates the number of different level of step sizes; σ_x^2 is the variance of an image block; $\Upsilon(.)$ indicates the complementary error function; and N is the number of cover signal points over which a single watermark bit is embedded. It can be seen that the variance of the lifting-based DWT coefficients is much lower than the DWT coefficients, which supports the use of a lifting-based method for cover image decomposition to design robust watermarking (Phadikar and Maity, 2011). We have performed our experimentation using the lifting-based 'haar' wavelet for image transformation due to its simplicity and ease of implementation, although other lifting based wavelets can also be used. The scheme uses the HL and LH subbands for watermark embedding. This selection of subbands is analogous to the use of middle frequency coefficients for embedding in the case of unitary transforms such as the discrete Fourier transform (DFT) and the discrete cosine transform (DCT) to create a good trade off between robustness and fidelity.

Step 3: Watermark Embedding: The watermark bit embedding is done using the following steps:

(1) *Generation of near-Orthogonal Dither*: The near-orthogonal dithers d_i, $i = 0, 1,.., M$ are generated based on Eq. (7). The length of d_i is equal to the number of wavelet coefficients used to embed a watermark symbol (m).
(2) *Watermark bit Insertion*: The message (m) is randomly (key dependently) selected and embedded by modulating group of wavelets coefficients of the HL and LH subbands. The qth watermarked wavelet coefficient $\tilde{X}^q$ is obtained using Eq. (9). After the watermark embedding, the inverse lifting is calculated, and the watermarked image is obtained.

4.2. Decoding process

The decoding process consists of the following steps:

Step 1: Perform Steps 2, 3(1) of the image encoding process on the received or possibly distorted image. The same step size (Δ) and keys are used to generate the dither for decoding that were used for encoding.

Step 2: Watermark Extraction: The message/symbol ($\hat{m}$) is extracted from the group of wavelet coefficients that are used during data embedding, using Eq. (10). After all messages are extracted, the extracted messages (m) are stored in their proper sequence according to the key used for the watermark embedding.

Step 3: Decoding of Watermark Bit: Based on the extracted symbols, the watermark bits are decoded and reversely permuted, i.e., spatially rearranged and then XORed with random bits to get the watermark ($\hat{W}$). The random bits are generated using the same secret key that was used for the watermark permutation at the encoder.

Step 4: Decoding Reliability for the Extracted Watermark: We calculate the normalized cross correlation (NCC) between the original watermark image (W) and the decoded watermark image ($\hat{W}$) to quantify the visual quality of the extracted watermark. The NCC is defined by Eq. (18) below.

$$\mathrm{NCC} = \frac{\sum_i \sum_j W_{ij}\hat{W}_{ij}}{\sum_i \sum_j (W_{ij})^2} \tag{18}$$

5. Performance evaluation

The performance of the proposed scheme is evaluated over 25 test images. However, the results are reported here only for six popular test images, namely Lena, Pepper, Baboon, Boat, Opera and Cameraman, having varied image characteristics (Test image source, xxxx). All of the test images are 8-bit gray scale images of size (512×512), and the experiments are conducted using a Pentium IV, 2.80 GHz processor, with 512 MB RAM using MATLAB 7. In this scheme, the image is decomposed into two levels using lifting, i.e., $n = 2$. This study uses the peak–signal-to-noise-ratio (PSNR) and the mean–structure-similarity-index-measure (MSSIM) (Wang and Bovik, 2004) as distortion measures for the watermarked image, where as the relative entropy distance (Kullback Leibler distance) (Maity et al., 2004) is used as measure of security (ε). The high PSNR & MSSIM values of the watermarked images and low security values indicate better imperceptibility and security of the hidden data, respectively.

MSSIM is defined as follows (Wang and Bovik, 2004):

$$MSSIM(P, \bar{P}) = \frac{1}{M'} \sum_{j'=1}^{M'} SSIM(P_{j'}, \bar{P}_{j'}) \tag{19}$$

where

$$SSIM(P, \bar{P}) = [l(P, \bar{P})]^{\delta}.[c(P, \bar{P})]^{\beta}.[s(P, \bar{P})]^{\gamma} \tag{20}$$

The functions $l(P, \bar{P})$, $c(P, \bar{P})$ and $s(P, \bar{P})$ are the luminance comparison, the contrast comparison and the structure comparison functions, respectively. The symbols δ, β and γ $\{\delta, \beta, \gamma > 0\}$ are the parameters used to adjust the relative importance of the components.

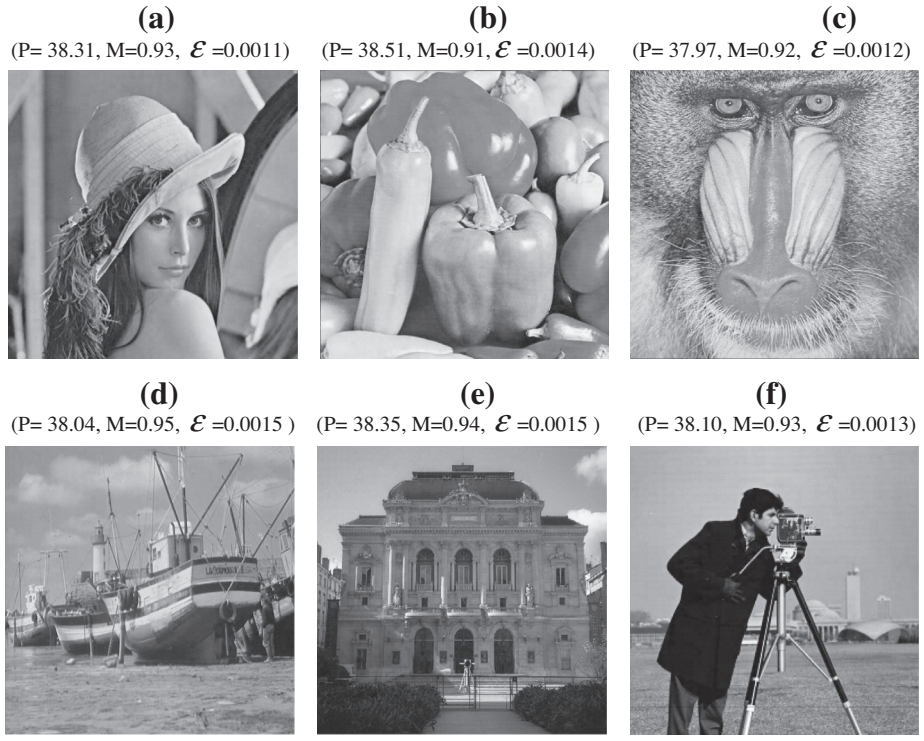

Figure 6 Watermarked images: (a) Lena, (b) Pepper, (c) Baboon, (d) Boat, (e) Opera, (f) Cameraman. (P, M, ε) above each image represents the PSNR (in dB), MSSIM and security values of the watermarked image.

Let the random variables R and S represent the original and the watermarked images, respectively. The Kullback Leibler distance $D(p||q)$ is defined as follows (Maity et al., 2004):

$$D(p||q) = \sum_{x \in X} p(x) \log \frac{p(x)}{q(x)} = E_p \log \frac{p(X)}{q(X)} \tag{21}$$

$$\text{with } 0 \log \frac{0}{q} = 0, p \log \frac{p}{0} = \propto$$

where $p(X)$ and $q(X)$ denote the probability distribution functions of the random variables R and S, respectively. The symbol E_p represents the expectation with respect to the joint distribution p. The value is always non-negative or zero (if $p(X) = q(X)$). If $D(p||q) \leqslant \varepsilon$, the security value may be assumed to be ε.

Fig. 6 shows the watermarked images along with the PSNR, MSSIM and ε values. Fig. 7(a) shows the original watermark image, while Fig. 7(b) shows the extracted watermark from all the watermarked images. Fig. 7(c) shows the extracted watermark with the fake key. Without the true key, the extracted signature looks like noise, which demonstrates that our scheme is sensitive to key (K) and hence is secured.

To test the robustness of the proposed watermarking scheme, some typical signal/image processing operations are performed. The robustness of the proposed scheme depends on the value of M, the step size (Δ) and the number of wavelet coefficients used for watermark bit embedding. For the image-scaling operation, before watermark extraction, the attacked images are rescaled to the original size. Down-sampling and up-sampling are carried out by bilinear interpolation. Initially, the host image is down-sampled by a factor of 0.75, and up-sampling is then done to the original size of the image. During simulation, it is performed by imresize functions available in the MATLAB. Table 2 lists the *NCC* values for different M-values. Table 3 lists the decoding time in seconds for different M-values. The numerical values in Table 2 and Table 3 are obtained as the average value of 100 independent experiments conducted over 25 benchmark images with varied image characteristics. Fig. 8 shows the average NCC performance under different compression ratios (for lossy JPEG compression) for different M-values. Each point on the curves is obtained as the average value of 100 independent experiments conducted over 25 benchmark images.

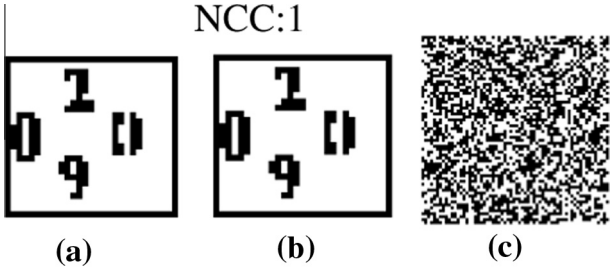

Figure 7 (a) Original watermark image (32×32); (b) Extracted watermark (32×32) from all watermarked image with NCC = 1; (c) Extracted watermark using fake key.

From Table 2 and Fig. 8, it is quite clear that with an increase in the M-value, the robustness efficiency is improved, but at the same time, the computation cost (time) of decoding is also increased (see Table 3). The reason for the latter point is that to decode a particular symbol, the watermarked data are projected onto all the dithers of that particular position. Gen-

Table 2 Robustness performance (NCC) for different M-value.

Strength	$M = 2$	$M = 4$	$M = 8$	$M = 16$
Median filtering (3 × 3)	0.8175	0.9202	0.9509	0.9737
Mean filtering (3 × 3)	0.8639	0.9290	0.9614	0.9705
Highpass filtering (1.8)	0.9635	0.9845	0.9930	0.9952
Down & Up sampling (0.75)	0.9270	0.9623	0.9825	0.9993
Histogram equalization	0.9314	0.8470	0.9930	0.9949
Dynamic range change (50–200)	0.9723	0.9889	0.9930	0.9982
Salt & pepper noise (0.05)	1	1	1	1
Speckle noise (0.05)	0.4790	0.5166	0.5223	0.5263
Gaussian noise (0.05)	0.5011	0.5322	0.5579	0.5719

Table 3 Decoding time in second for different M-value.

$M = 2$	$M = 4$	$M = 8$	$M = 16$
12.07	22.56	46.26	97.15

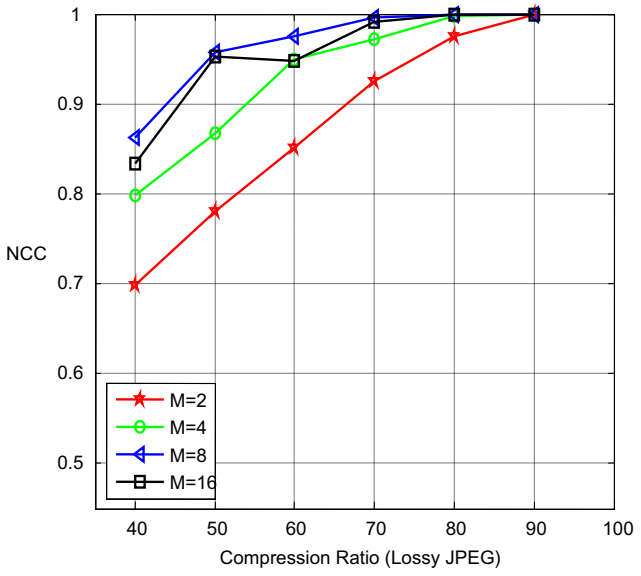

Figure 8 NCC performance of different M-values under lossy JPEG compression.

erally, for a large M-value, the complexity for decoding the watermark bit increases exponentially, i.e., $O(2^N)$. It may be noted that the parallel implementation of M-ary amplitude modulation is computationally effective. Compared to a conventional decoder of M-ary QIM, the simulation time with the parallel implementation of the decoder could reach $1/2^N$. Moreover, from Table 2 and Table 3, it is also clear that for an increase of the M-value from 8 to 16, the robustness performance is not increased significantly, while the decoding time is increased significantly. This, in other words, signifies that the decoding complexity of the higher M-values can be overcome at moderate N-values, while robustness performance is maintained at a satisfactory level. The robustness performance is also tested against geometric attacks such as slight rotations, as the QIM-based scheme is usually vulnerable in that regard.

Table 4 Experimental results with Stirmark 4.0 for $M = 16$.

Strength	NCC	Strength	NCC
Median filtering (3 × 3)	0.97	LATESTRNDDIST_1	0.95
Median filtering (5 × 5)	0.97	LATESTRNDDIST_1.05	0.94
Median filtering (7 × 7)	0.96	Remov_lines_10	1.00
Rotation-scaling 0.25	0.93	Remov_lines_50	0.99
Rotation-scaling-0.25	1.00	Remov_lines_70	1.00
Rotation-cropping 0.25	1.00	Remov_lines_100	1.00
Rotation-cropping −.25	1.00	JPEG_80	1.00
Rotation _0.25	1.00	JPEG_50	0.97
Rotation _5	1.00	Cropping_50	1.00
Rotation _90	1.00	CONV_1	0.86

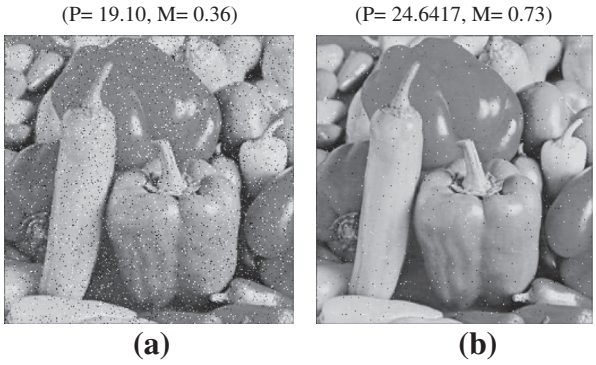

Figure 9 Watermarked images after passing through fading channel (a): SNR = 3, (b): SNR = 7. (P, M) above each image represents the PSNR (in dB) and MSSIM values of the image.

Table 5 BER (bit error rate) of the extracted watermark bits for different channel SNR (dB) and M values.

SNR(dB)	−15	−10	−5	−3	−1	1	3
$M = 2$	0.41	0.35	0.27	0.08	0.06	0	0
$M = 4$	0.30	0.20	0.12	0.06	0.04	0	0
$M = 8$	0.20	0.15	0.10	0.04	0	0	0
$M = 16$	0.08	0.05	0.02	0.01	0	0	0

For the rotation operation, we have estimated the rotation angle of the watermarked images by the control point selection method with the help of the original images. The rotated watermarked images are then inversely rotated and corrected by linear interpolation. Now, those corrected watermarked images are used for watermark detection. This process is performed to compensate for the effect of loss in data due to the rotation operation. Table 4 lists the experimental results using the benchmark StirMark 4.0 (Petitcolas, 2000). From Table 4, it is clear that the proposed scheme is not only robust for common image processing operations but also against geometric attacks.

To show the effectiveness of the proposed data hiding method over a fading channel, we simulate our test for different channel condition. Data transmission is accomplished using multi carrier code division multiple access (MC-CDMA)

Table 6 Comparison of results for PSNR (dB) and NCC values under various attack methods. Number of watermark bits is 1024.

Attack method	Mohan et al. (2008)	Zaghlou and Rawashdeh (2008)	Kumsawat et al. (2007)	Proposed $M = 16$
Lowpass filtering (3 × 3)	0.49	0.82	0.69	0.97
Median filtering (3 × 3)	0.78	0.84	0.64	0.97
JPEG-80	1.00	0.93	1.00	1.00
JPEG-75	1.00	0.81	0.99	0.99
JPEG-50	0.96	0.79	0.90	0.97
Rotation 10 degree	0.74	0.97	0.65	1.00
Down & Up sampling 0.75	0.82	0.73	–	0.99
Cropping 10%	0.89	0.81	0.95	1.00

(Maity and Mukherjee, 2009) through a Rayleigh fading wireless channel with various channel signal-to-noise-ratios (SNR). In this simulation, we have used a four-ray frequency selective slow Rayleigh fading model (Natarajan et al., 2000). A small value of SNR represents that the channel is under deep fade, while a high value of SNR represents the reverse. Fig. 9 shows the images after passing through the fading channel with different channel SNR. The bit error rate (BER) of the extracted watermark for different signal-to-noise-ratios (SNR) of Rayleigh fading wireless channels are shown in Table 5. It is seen that the bit error rate (BER) is decreased with the increase in M-values. BER here denotes the error in the extracted watermark bits passing through the fading channel.

The robustness performance of the proposed method is also compared with previously reported work (Mohan et al., 2008; Zaghlou and Rawashdeh, 2008; Kumsawat et al., 2007) to demonstrate the performance comparison. It is observed from the results of Table 6 that the proposed method offers better gain in term of NCC, which is due to the use of M-ary QIM for multibit data embedding.

6. Conclusions and scope of future work

This paper critically analyzes the use of the M-ary amplitude modulation principle in multibit QIM watermarking with the integration of lifting. The simulation results show that the robustness is maintained at a satisfactory level using moderate M-values. Moreover, the experimental results also show that our scheme is highly robust against several image processing operations, which include filtering, cropping, scaling, compression, geometric attacks such as rotation, the random removal of some row and column lines, the addition of various noises and transmission through a fading channel. Future work can be expected to concentrate on the further performance improvement of the proposed scheme and the reduction of the computation load (time) in data extraction to a very low level, as well as the development of a hardware implementation of the proposed scheme through a field-programmable gate array (FPGA).

References

Adams, M.D., Kossentini, F., 2000. Reversible integer-to-integer wavelet transforms for image compression: performance evaluation and analysis. IEEE Transaction on Image Processing 9, 1010–1024.

Boliek, M., Christopoulos, C., Majani, E., 2000. JPEG 2000 Part I Final Draft International Standard. ISO/IEC FDIS15444-1, ISO/IEC JTC1/SC29/ WG1 N1855.

Calderbank, A.R., Daubechies, I., Sweldens, W., Yeo, B.L., 1998. Wavelet transforms that map integers to integers. Applied and Computational Harmonic Analysis 5, 332–369.

Chen, B., Wornell, G.W., 2001. Quantization index modulation: a class of provably good methods for digital watermarking and information embedding. IEEE Transaction of Information Theory 47, 1423–1443.

Claypoole, R.L., Baraniuk, R.G., Nowak, R.D., 1998. Adaptive wavelet transforms via lifting. In: Proc. IEEE International Conference on Acoustics, Speech and Signal Processing, Seattle, WA.

Costa, M., 1983. Writing on dirty paper. IEEE Transactions on Information Theory 29, 439–441.

Gonzalez, F.P., Mosquera, F., Barni, M., Abrardo, A., 2005. Rational dither modulation: a high-rate data-hiding method invariant to gain attacks. IEEE Transactions on Signal Processing, Supplement on Secure Media 53 (10), 3960–3975.

Kumsawat, P., Attakitmongcol, K., Srikaew, A., 2007. A robust image watermarking scheme using multiwavelet tree. In: Proc. of the World Congress on Engineering, London, UK.

Maity, S.P., Mukherjee, M., 2009. Subcarrier PIC scheme for high capacity CI/MC-CDMA system with variable data rates. In: Proc. of IEEE Mobeile WiMAX, Canada.

Maity, S.P., Nandy, P., Das, T.S., Kundu, M.K., 2004. Robust image watermarking using multiresolution analysis. In: Proc. of the IEEE INDICON, India.

Maity, S.P., Kundu, M.K., Das, T.S., 2005. Robust SS watermarking with improved capacity. Pattern Recognition Latter 28, 300–357.

Mohan, B.C., Srinivaskumar, S., Chatterji, B.N., 2008. A robust digital image watermarking scheme using singular value decomposition (SVD), dither quantization and edge detection. Journal ICGST-GVIP 8, 17–23.

Natarajan, B., Nassar, C., Chandrasekhar, V., 2000. Generation of correlated Rayleigh fading envelopes for spread spectrum applications. IEEE Communication Letter 4 (1), 9–11.

Petitcolas, F.A.P., 2000. Watermarking schemes evaluation. IEEE Signal Processing 17, 58–64.

Phadikar, A., Maity, S.P., 2010. Multibit QIM watermarking using M-Ary modulation and lifting. Proceedings of the International Conference on Signal Processing and Communications, Bangalore.

Phadikar, A., Maity, Santi P., 2011. Data hiding based quality access control of digital images using adaptive QIM and lifting. Journal of Signal Processing: Image Communication 26 (10), 646–661.

Phadikar, A., Maity, S.P., Kundu, M.K., 2008. Quantization based data hiding scheme for efficient quality access control of images using DWT via lifting. In: Proc. of the 6th IEEE Indian Conference on Computer Vision, Graphics and Image Processing, Bhubaneswar, India.

Test image source. < www.petitcolas.net > .

Uytterhoeven, G., Roose, D., Bultheel, A., 1997. Wavelet Transforms using Lifting Scheme. Technical Report ITA-Wavelets Report WP

1.1, Katholieke Universiteit Leuven, Department of Computer Science, Belgium.

Voloshynovskiy, S., Pun, T., 2002. Capacity security analysis of data hiding technologies. In: Proc. IEEE International Conference on Multimedia and Expo, Lausanne, Switzerland.

Wang, Z., Bovik, A.C., Sheikh, H.R., Simoncelli, E.P., 2004. Image quality assessment: from error measurement to structural similarity. IEEE Transactions on Image Processing 13, 1–14.

Xin, Y., Pawlak, M., 2008. M-ary phase modulation for digital watermarking. International Journal of Applied Mathematics and Computer Science 18 (1), 93–104.

Zaghlou, R.I., Rawashdeh, E.F.A., 2008. HSV image watermarking scheme based on visual cryptography. World Academy of Science, Engineering and Technology 44, 482–485.

Amit Phadikar received his PhD degree in Information Technology in 2011 from BESU, Shibpur, India. Presently he is working as Associate Professor in the Department of IT, MCKVIE, Liluah, India. His research areas include digital image and signal processing. He has contributed two books and about 40 research papers in reputed journals and conferences.